

# Bottom-up Policy Optimization: Your Language Model Policy Secretly Contains Internal Policies

Yuqiao Tan <sup>\*1 2</sup> Minzheng Wang <sup>\*1 2</sup> Shizhu He <sup>1 2 †</sup> Huanxuan Liao <sup>1 2</sup> Chengfeng Zhao <sup>1 2</sup> Qiunan Lu <sup>3</sup>  
 Tian Liang <sup>4</sup> Jun Zhao <sup>1 2</sup> Kang Liu <sup>1 2</sup>  
 <https://github.com/TraelounG/BuPO>

## Abstract

Existing reinforcement learning (RL) approaches treat large language models (LLMs) as a unified policy, overlooking their internal mechanisms. In this paper, we decompose the LLM-based policy into **Internal Layer Policies** and **Internal Modular Policies** via Transformer’s residual stream. Our entropy analysis on internal policy reveals distinct patterns: (1) universally, policies evolve from high-entropy exploration in early layers to deterministic refinement in top layers; and (2) Qwen exhibits a progressive, human-like reasoning structure, contrasting with the abrupt final-layer convergence in Llama. Furthermore, we discover that optimizing internal layers induces feature refinement, forcing lower layers to capture high-level reasoning representations early. Motivated by these findings, we propose **Bottom-up Policy Optimization (BuPO)**, a novel RL paradigm that reconstructs the LLM’s reasoning foundation from the bottom up by optimizing internal layers in early stages. Extensive experiments on complex reasoning benchmarks demonstrate the effectiveness of BuPO.

## 1. Introduction

Reinforcement learning (RL) has emerged as a key driver in advancing the complex reasoning capabilities of large language models (LLMs) (Ouyang et al., 2022; Jaech et al., 2024). Notably, the success of DeepSeek-R1 (Guo et al., 2025) has solidified reinforcement learning with verifiable rewards (RLVR) as a potent post-training paradigm

<sup>\*</sup>Equal contribution, <sup>†</sup>Corresponding author <sup>1</sup>Institute of Automation, Chinese Academy of Sciences <sup>2</sup>University of Chinese Academy of Sciences <sup>3</sup>University of Electronic Science and Technology of China <sup>4</sup>Tencent AI Lab. Mails to: tanyuqiao2025@ia.ac.cn, wangminzheng2023@ia.ac.cn, shizhu.he@nlpr.ia.ac.cn.

Preprint. February 3, 2026.

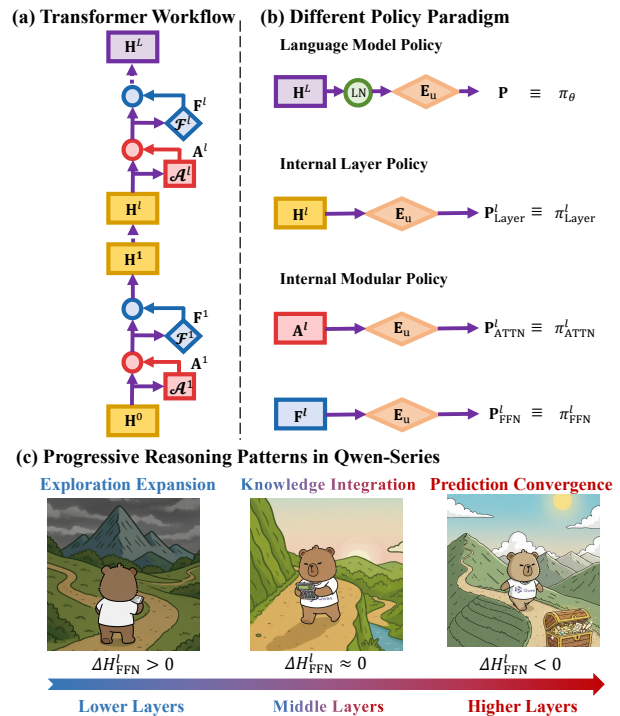


Figure 1. (a): The residual stream within Transformer moves from previous layer into self-attention and feed-forward network (FFN) sequentially. (b): Any hidden states with unembedding matrix  $E_u$  can be transformed into probability distribution  $P$  over the vocabulary space, which can be considered as a policy. (c): We surprisingly find that Qwen-series contains a progressive reasoning pattern in FFN, where it starts from exploration expansion to integrate middle layer knowledge into final prediction convergence.

for enhancing language model policy across diverse domains (Yang et al., 2025; Team et al., 2025; Yu et al., 2025). However, existing RL approaches typically treat the LLM as a unified policy, optimizing it solely on the final output distribution while neglecting the intricate information flow evolving through its internal residual streams. Mechanistic interpretability tools mitigate the opacity of black-box LLMs by unveiling their internal logic (Belrose et al., 2023; Tan et al., 2025a; Gupta et al., 2025). Such insights are viewed as a crucial bridge between deeper understanding of

internal behavior and principled algorithmic refinement.

While recent works leverage the attention mechanisms to improve RL algorithm (Li et al., 2025; Liu et al., 2025), they overlook the nature of the language model policy as well as the information latent in the residual stream. The logit lens (nostalgia, 2020) framework offers initial insights by employing the unembedding matrix  $\mathbf{E}_u$  to decode intermediate layer representations into the token space. This approach reveals that the internal residual stream harbors a wealth of undiscovered information that evolves across layers and modules (Dai et al., 2022; Gupta et al., 2025; Lindsey et al., 2025). Moreover, numerous studies have elucidated the mechanisms of self-attention and feed-forward network (FFN) (Dai et al., 2022; Yu & Ananiadou, 2024; Jin et al., 2025). Collectively, these mechanisms within models offer a new perspective for algorithmic optimizations.

In this paper, we investigate the evolution of language model policies across layers and modules to facilitate optimization and unravel complex internal reasoning mechanisms. Our formulation is grounded in two key insights. First, the residual stream naturally supports additive decomposition (Zhang et al., 2025; Lindsey et al., 2025), allowing us to isolate the individual roles of each layer and module (Figure 1(a)). Second, we conclude that the samplable policy is intrinsic equivalent to the token distribution derived from the combination of hidden states  $\mathbf{H}$  with unembedding matrix  $\mathbf{E}_u$ . Based on these, we construct the **Internal Layer Policy**  $\pi_{\text{Layer}}^l$ , which captures cumulative reasoning up to layer  $l$ , and the **Internal Modular Policy**  $\pi_{\text{ATTN}}^l$  and  $\pi_{\text{FFN}}^l$ , which isolates the specific contributions of attention and FFN modules (Figure 1(b)). This decomposition allows us to ask: *How does internal reasoning evolve through the model?*

Through systematic analysis of commonly used Qwen and Llama series (Meta AI, 2024; Yang et al., 2024; 2025) based on **Internal Policy Entropy** in a policy-centric view, we uncover both universal and critical architectural differences: **(1) Consistent internal reasoning structure.** All models exhibit a universal reasoning structure: early layers maintain high entropy for exploring the solution space, while top layers converge to near-zero for final prediction (Lindsey et al., 2025). **(2) Distinct internal reasoning pattern.** Despite the shared trend, the pace of convergence differs significantly. Llama exhibits a sudden convergence only within the last three layers. In contrast, Qwen models demonstrate a progressive contraction, gradually reducing uncertainty throughout layers. To quantify these dynamics, we introduce **Entropy Change**. This metric reveals that while Llama shows minimal internal updates, Qwen utilizes FFN in a progressive, human-like cognitive process (Dehaene et al., 1998): expanding exploration in lower layers, integrating parametric knowledge in intermediate layers, and compacting predictions in upper layers (Figure 1(c)).

These findings have profound implications for RL optimization: *Since internal reasoning emerges progressively from lower to higher, we can consider optimization from a bottom-up perspective.* We initially validate this hypothesis through targeted optimization on internal policies, revealing distinct training dynamics and a remarkable phenomenon of internal reasoning feature refinement. Specifically, the optimized lower layers capture high-level reasoning capabilities by early alignment, providing a more robust foundation for subsequent internal reasoning. Motivated by these insights, we propose **Bottom-up Policy Optimization (BuPO)**, a novel RL paradigm that optimizes fine-grained internal layer policies during the early stages of training to effectively guide the overall language model policy. By doing so, BuPO reconstructs foundational reasoning abilities and achieves superior performance. Extensive experiments on complex reasoning benchmarks demonstrate the effectiveness of our approach and the unique training dynamics compared to conventional RL methods that optimize the policy as a whole.

In summary, this paper makes the following contributions: (1) We are the first to decompose an LLM policy into internal layer and modular policies, revealing their distinct roles in reasoning. (2) We reveal a universal exploration-to-convergence shift, distinguishing Qwen’s progressive reasoning from Llama’s abrupt convergence. Moreover, we uncover a feature refinement phenomenon where internal optimization drives lower layers to preemptively capture high-level features. (3) We propose BuPO to align internal policies from the bottom up, which reconstructs the foundational reasoning capabilities at lower layers, achieving superior performance on complex reasoning benchmarks.

## 2. Preliminary

In this section, we aim to introduce the basic definition helps to understand the decomposition of language model policy.

### 2.1. The Residual Stream in Transformer

Transformer-based language models (Vaswani et al., 2017) form the foundation of modern LLMs (Brown et al., 2020). A decoder-only Transformer consists of  $L$  stacked layers, each containing a multi-head self-attention (MHSA) module and a feed-forward network (FFN) module.

Following Zhang et al. (2025), we formalize the forward process from input to output. Given an input sequence  $\mathbf{x} = [x_1, x_2, \dots, x_T]$ , the model produces a probability distribution  $\mathbf{P}$  over the vocabulary  $V$  with  $N$  tokens. Let  $\mathbf{H}^{(2l-2)} \in \mathbb{R}^{T \times d_{\text{model}}}$  denote the hidden state input to the  $l$ -th layer, where  $T$  is the sequence length and  $d_{\text{model}}$  is the hidden dimension. The initial embedding is  $\mathbf{H}^{(0)}$  projected by  $\mathbf{E}$ , where  $\mathbf{E} \in \mathbb{R}^{N \times d_{\text{model}}}$  is the embedding matrix.

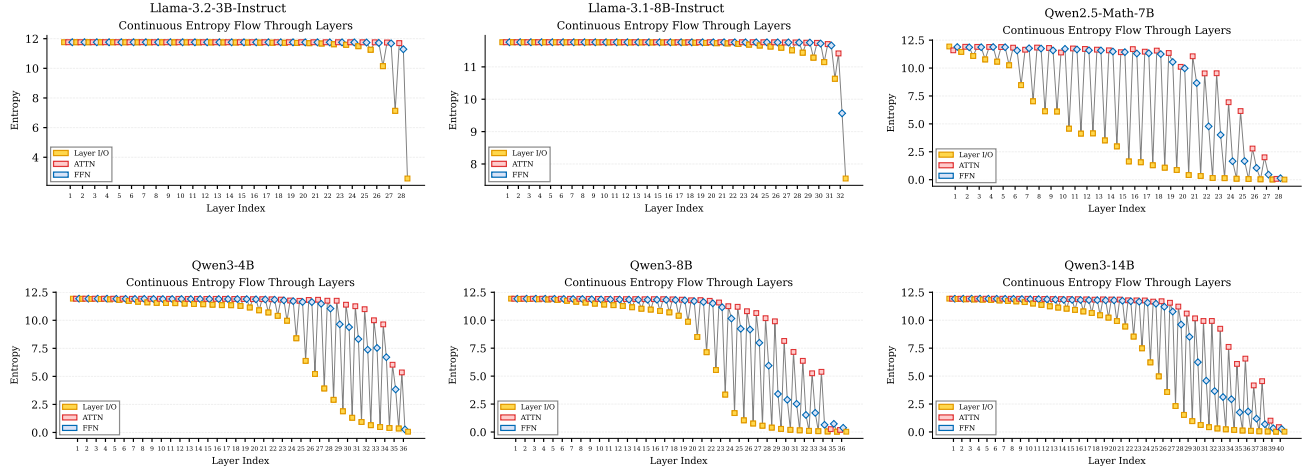


Figure 2. Continuous entropy dynamics of internal policy. The residual stream flows from  $\mathbf{H}^{l-1}$  into  $\mathbf{A}^l$ ,  $\mathbf{F}^l$ , then to the next layer  $\mathbf{H}^l$ .

Each layer forwards sequentially through attention and FFN:

$$\begin{aligned} \mathbf{A}^l &= \text{MHSA}(\text{LN}(\mathbf{H}^{(2l-2)})), \quad \mathbf{H}^{(2l-1)} = \mathbf{H}^{(2l-2)} + \mathbf{A}^l, \\ \mathbf{F}^l &= \text{FFN}(\text{LN}(\mathbf{H}^{(2l-1)})), \quad \mathbf{H}^{(2l)} = \mathbf{H}^{(2l-1)} + \mathbf{F}^l, \end{aligned} \quad (1)$$

where  $\text{LN}(\cdot)$  denotes layer normalization, and  $\mathbf{A}^l$ ,  $\mathbf{F}^l$  represent the attention and FFN outputs, respectively.

After  $L$  layers, the final hidden states are projected to vocabulary logits:

$$\mathbf{P} = \text{softmax}(\text{LN}(\mathbf{H}^{(2L)})\mathbf{E}_u^T), \quad (2)$$

where  $\mathbf{E}_u \in \mathbb{R}^{N \times d_{\text{model}}}$  is the unembedding matrix, and  $\mathbf{P} \in \mathbb{R}^{T \times N}$  denotes the output probability distribution.

## 2.2. Reinforcement Learning for Language Model Policy

Language model generation can be formulated as a token-level Markov Decision Process (MDP). At each step  $t$ , the state  $s_t = [\mathbf{q}; \mathbf{o}_{<t}]$  consists of the input question and generated tokens so far. The language model policy  $\pi_\theta(\cdot|s_t)$  samples the next token  $o_t$  from vocabulary  $V$ , transitioning to  $s_{t+1} = [s_t; o_t]$ . Generation terminates upon producing  $[\text{eos}]$  or reaching the budget.

To optimize the policy, we maximize:

$$\begin{aligned} \mathcal{J}(\pi_\theta) &= \\ &\mathbb{E}_{\mathbf{q} \sim \mathcal{Q}} \left[ \mathbb{E}_{\mathbf{o} \sim \pi_\theta(\cdot|\mathbf{q})} [R(\mathbf{q}, \mathbf{o})] - \beta \mathbb{D}_{KL}[\pi_\theta(\cdot|\mathbf{q}) || \pi_{\text{ref}}(\cdot|\mathbf{q})] \right], \end{aligned} \quad (3)$$

where  $R(\mathbf{q}, \mathbf{o}) = \sum_{t=1}^{|\mathbf{o}|} r(s_t, o_t)$  is the return (Sutton et al., 1998) and  $\pi_{\text{ref}}$  is a reference policy. We adopt sparse rewards where  $r_t = 0$  for  $t < n$  and  $r_n \in [0, 1]$  indicates task success. Following Hu et al. (2025a), we assume  $\beta = 0$ .

**Policy Optimization.** We adopt GRPO (Shao et al., 2024), which samples a group of responses  $\{\mathbf{o}_1, \dots, \mathbf{o}_G\}$  per question and estimates advantages as  $\hat{A}_{i,t} = \frac{R_i - \text{mean}(\mathbf{R})}{\text{std}(\mathbf{R})}$ :

$$\begin{aligned} \mathcal{J}_{\text{GRPO}}(\pi_\theta) &= \mathbb{E}_{\mathbf{q} \sim \mathcal{Q}, \{\mathbf{o}_i\}_{i=1}^G \sim \pi_{\theta_{\text{old}}}(\cdot|\mathbf{q})} \\ &\frac{1}{G} \sum_{i=1}^G \frac{1}{|\mathbf{o}_i|} \sum_{t=1}^{|\mathbf{o}_i|} \left\{ \min \left[ r_{i,t} \hat{A}_{i,t}, \text{clip}(r_{i,t}, 1 - \epsilon, 1 + \epsilon) \hat{A}_{i,t} \right] \right\}, \end{aligned} \quad (4)$$

where  $r_{i,t} = \frac{\pi_\theta(o_{i,t} | s_{i,t})}{\pi_{\theta_{\text{old}}}(o_{i,t} | s_{i,t})}$  is the importance ratio.

## 3. Language Model Policy Secretly Contains Internal Policies

In this section, we introduce our key insight: *the language model policy secretly contains internal policies*. We provide implementation details of this section in Appendix A.4.

### 3.1. Definition of Internal Policy

**Residual Stream.** In the residual stream of Transformer, the input to any layer equals the sum of all preceding outputs plus the original embedding. The hidden states satisfy:

$$\mathbf{H}^l = \mathbf{H}^{(2l)} = \mathbf{H}^{(0)} + \sum_{i=1}^l \mathbf{A}^i + \sum_{j=1}^l \mathbf{F}^j, \quad (5)$$

where we denote  $\mathbf{H}^l$  for simplicity as the output hidden states in layer  $l$  same as  $\mathbf{H}^{(2l)}$ . According to this, the output of final layer can be regard as the combination of previous hidden states by  $\mathbf{H}^L = \mathbf{H}^0 + \sum_{i=1}^L \mathbf{A}^i + \sum_{j=1}^L \mathbf{F}^j$ .

**Internal Policy.** During RL, we sample the next token  $o_t$  from the final layer's probability distribution, i.e.,  $\pi_\theta = \mathbf{P} = \text{softmax}(\text{LN}(\mathbf{H}^L)\mathbf{E}_u^T)$ . We propose that every internal

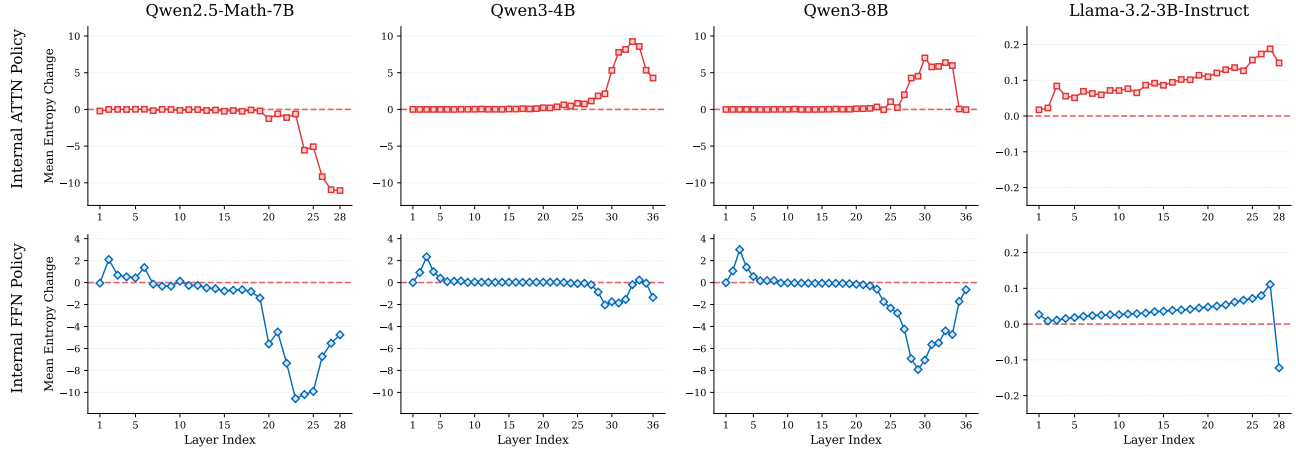


Figure 3. Entropy change dynamics of internal policy. The entropy change  $\Delta H^l$  across layers represents the uncertainty of current policy’s hidden exploration space. A positive  $\Delta H^l > 0$  indicates increasing exploration,  $\Delta H^l \approx 0$  signifies exploitation of existing knowledge, and  $\Delta H^l < 0$  suggests a tendency toward convergence within the reasoning process.

hidden states can combine with  $\mathbf{E}_u$  to produce a samplable policy. Specifically, we focus on two granularities. **Internal Layer Policy** refers to utilize hidden states from each layer  $\mathbf{H}^l$  to combine with  $\mathbf{E}_u$ , and **Internal Modular Policy** integrates  $\mathbf{E}_u$  with hidden states from specific module:

$$\pi_{\text{Layer}}^l \equiv \mathbf{P}_{\text{Layer}}^l = \text{softmax}(\mathbf{H}^l \mathbf{E}_u^T), \quad (6)$$

$$\pi_{\text{Module}}^l \equiv \begin{cases} \mathbf{P}_{\text{ATTN}}^l = \text{softmax}(\mathbf{A}^l \mathbf{E}_u^T), & \text{for ATTN} \\ \mathbf{P}_{\text{FFN}}^l = \text{softmax}(\mathbf{F}^l \mathbf{E}_u^T). & \text{for FFN} \end{cases} \quad (7)$$

Each component contributes to the final policy through the residual stream. For instance,  $\mathbf{H}^L = \mathbf{H}^l + \mathbf{S}^{l+1}$ , where  $\mathbf{S}^{l+1} = \sum_{i=l+1}^L \mathbf{A}^i + \sum_{j=l+1}^L \mathbf{F}^j$  represents contributions from subsequent layers. Hence, understanding these internal components is essential for unraveling *how internal reasoning emerge and evolve through the model*.

### 3.2. Internal Policy Entropy Dynamics

In contrast to prior logit lens approaches (nostalgia, 2020; Belrose et al., 2023) that decode internal states into discrete tokens, we adopt a policy-centric perspective where internal probability distributions are treated as policies. We employ **Entropy** as our primary metric, motivated by its strong correlation with policy behavior (Cui et al., 2025; Cheng et al., 2025). We define **Internal Policy Entropy** as:

$$H_{\text{Layer}}^l = - \sum_{j=1}^{|V|} \mathbf{P}_{\text{Layer},j}^l \cdot \log(\mathbf{P}_{\text{Layer},j}^l), \quad (8)$$

where  $|V|$  denotes the vocabulary size and we can obtain  $H_{\text{FFN}}^l$  and  $H_{\text{ATTN}}^l$  in the same way.

**Continuous Entropy Dynamics.** Figure 2 shows that internal policy entropy dynamics exhibit consistent patterns

across models: early layers maintain high entropy for exploration of the search space, while top layers converge to near-zero entropy. This aligns with findings that lower layers capture semantic information while higher layers aggregate and refine these representations to drive final decision-making (Lindsey et al., 2025).

While the overall entropy pattern is consistent across models, the fine-grained transition dynamics vary. To isolate intrinsic patterns from normalization and residual effects (He et al., 2016; Zhang & Sennrich, 2019), we introduce **Entropy Change**, which measures the incremental information gain within a single internal policy and is defined as:

$$\Delta H^l = H_{\text{Output}}^l - H_{\text{Input}}^l, \quad (9)$$

where the entropy change is defined as the difference between the internal policy entropy at a module’s input and output. This metric reveals how the exploration space evolves as information propagates through the specific module.

**Entropy Change Dynamics of Attention vs. FFN.** *Self-attention* modules (Vaswani et al., 2017) are widely regarded as central to model reasoning, particularly for integrating task-relevant contextual information (Jin et al., 2025; Liu et al., 2025). The upper panel of Figure 3 reveals a clear and model-dependent pattern in the entropy change of self-attention. Specifically, Qwen3 models exhibit consistently positive entropy change across layers ( $\Delta H_{\text{ATTN}}^l > 0$ ), indicating sustained expansion of the exploration space during reasoning, consistent with prior findings (Li et al., 2025; Lindsey et al., 2025; Zhou et al., 2025). In contrast, Qwen2.5-Math-7B shows uniformly negative entropy change, suggesting progressive contraction and earlier convergence. Llama models display a weaker but still positive trend, reflecting more conservative exploration dynamics.

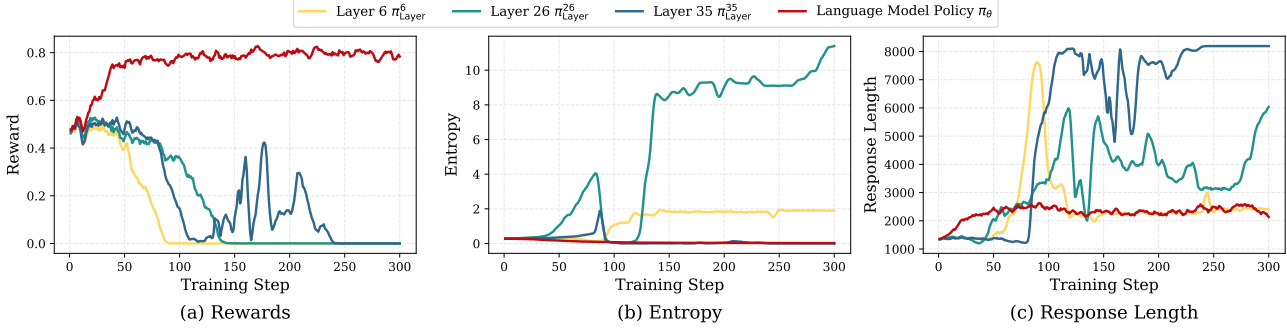


Figure 4. Training dynamics of internal policy. Effects of varying the optimized policy on (a) reward, (b) entropy of language model policy  $\pi_{\theta}$ , (c) response length. The backbone model is Qwen3-4B.

Moreover, the *FFN* module is widely regarded as the key-value memories of parametric knowledge (Geva et al., 2021; Meng et al., 2022; Dai et al., 2022). The lower panel of Figure 3 reveals clear and systematic differences in FFN entropy dynamics across model families. For the Llama models (Meta AI, 2024), FFN entropy remains consistently positive across almost all layers, with convergence occurring only at the final layer. This pattern indicates sustained but weak exploration throughout the FFN, which aligns with prior observations that Llama models benefit less from post-training and require additional mid-training interventions to improve reasoning behavior (Wang et al., 2025b).

By contrast, the Qwen models (Yang et al., 2024; 2025) exhibit a pronounced hierarchical entropy structure in the FFN, following a clear three-stage progression. Taking Qwen3-4B as an example, the lower FFN layers (layers 1-6) show increased entropy ( $\Delta H_{\text{FFN}}^l > 0$ ), corresponding to expanded exploration at the onset of reasoning. Followed by a broad middle region (layers 7-26) where  $\Delta H_{\text{FFN}}^l \approx 0$ , indicating stable information integration through retrieval and reuse of parametric knowledge (Dai et al., 2022). In the upper layers (layers 27-36),  $\Delta H_{\text{FFN}}^l < 0$ , reflecting gradual convergence toward the final prediction.

Notably, this Exploration–Integration–Convergence (EIC) pattern is more consistently expressed in Qwen3 than in earlier Qwen2.5 variants, indicating a more structurally stabilized and progressive reasoning pattern. We hypothesize that this progressive reasoning pattern, qualitatively similar to the staged nature of human reasoning (Dehaene et al., 1998; Yamins & DiCarlo, 2016), may help explain why Qwen3 exhibits more efficient knowledge absorption during post-training (Zhu et al., 2025; Yang et al., 2025). The analysis of residual stream similarity in Appendix B.2 further supports our finding in EIC pattern.

## 4. Internal Policy Optimization

Building on previous analysis, we observe that internal reasoning emerges progressively, with different internal policy

regions serving distinct roles and exhibiting varied behaviors. This raises a key question: *Can we approach bottom-up optimization to align with this progressive emergence?* To address this, we extend GRPO which designed for language model policy to directly optimize these internal policies:

$$\mathcal{J}_{\text{InterGRPO}}(\pi_{\theta}, \pi_{\text{Layer}}^l) = \mathbb{E}_{\mathbf{q} \sim \mathcal{Q}, \{\mathbf{o}_i\}_{i=1}^G \sim \pi_{\theta_{\text{old}}}(\cdot | \mathbf{q})} \frac{1}{G} \sum_{i=1}^G \frac{1}{|\mathbf{o}_i|} \sum_{t=1}^{|\mathbf{o}_i|} \left\{ \min \left[ \hat{r}_{i,t} \hat{A}_{i,t}, \text{clip}(\hat{r}_{i,t}, 1 - \epsilon, 1 + \epsilon) \hat{A}_{i,t} \right] \right\}, \quad (10)$$

where we sample from  $\pi_{\theta_{\text{old}}}$  and  $\hat{r}_{i,t} = \frac{\pi_{\text{Layer}}^l(o_{i,t} | \mathbf{q}, \mathbf{o}_{i,<t})}{\pi_{\text{Layer},\text{old}}^l(o_{i,t} | \mathbf{q}, \mathbf{o}_{i,<t})}$  for current optimizing policy  $\pi_{\text{Layer}}^l$  and keep other designs same with Eq. 4. We use Qwen3-4B as the backbone and present the implementation details in Appendix A.5.

**Different Training Dynamics of Internal Policy.** As shown in Figure 4, both internal layer policies collapse after 50 training steps. Nevertheless, distinct patterns emerge. For the penultimate layer policy  $\pi_{\text{Layer}}^{35}$ , entropy shows minor fluctuations before aligning with  $\pi_{\theta}$ . But it suffers from repetition causing excessively long responses, likely because final decision-making is confined to the last layer (Gupta et al., 2025). In contrast, the last integration region policy  $\pi_{\text{Layer}}^{26}$  exhibits unstable and increased entropy. And the last exploration region policy  $\pi_{\text{Layer}}^6$  maintains stable entropy growth, with response lengths converging closer to  $\pi_{\theta}$ .

**Analysis of Internal Policy Optimization.** We further investigate the underlying mechanism of internal policy optimization. Surprisingly, we find that this process induces a significant feature refinement in the model’s internal states. Taking  $\pi_{\text{Layer}}^6$  for illustration, Figure 5 (a) shows that as optimization progresses, the similarity between its hidden states  $\mathbf{H}^6$  and the final layer representations increases. This suggests that internal optimization forces the bottom layer to preemptively capture high-level reasoning information, providing a more robust foundation for subsequent internal reasoning. While the entropy change dynamics in Figure 5(b) indicate that the optimized internal policy progressively con-

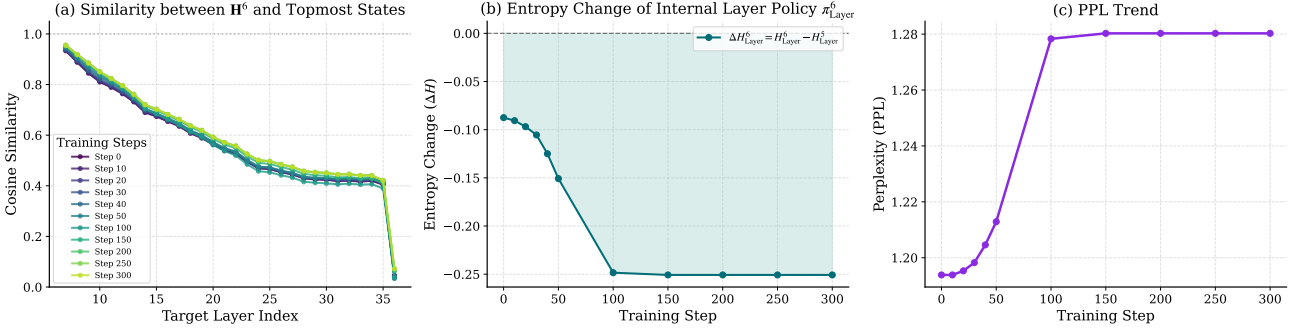


Figure 5. Analysis of internal policy optimization. (a) Similarity between the hidden states of optimized layer 6 and the higher layers. (b) Entropy Change  $\Delta H_{\text{Layer}}^6$  of the optimized  $\pi_{\text{Layer}}^6$ . (c) The PPL trend of the language model policy  $\pi_\theta$ . The backbone model is Qwen3-4B.

verges, the PPL trend in Figure 5(c) reveals a clear trade-off: excessive alignment leads to performance collapse, suggesting limited steps of optimization are optimal.

## 5. Bottom-up Policy Optimization

All prior RL methods for LLMs optimize the language model policy in a holistic manner (Ouyang et al., 2022; Rafailov et al., 2023; Guo et al., 2025). In Sec. 3, we decompose the final output  $\mathbf{H}^L$  into an intermediate representation  $\mathbf{H}^l$  and the subsequent residual contribution  $\mathbf{S}^{l+1}$ . This decomposition suggests that aligning the internal policy  $\pi_{\text{Layer}}^l$  associated with  $\mathbf{H}^l$  may facilitate alignment of the overall policy  $\pi_\theta$ . We empirically support this intuition in Sec. 4, where we optimize the internal policy alone and observe pronounced feature refinement in lower layers. These findings further motivate a bottom-up alignment strategy: by aligning fine-grained internal policies first, we explore whether the overall policy can be guided to reason more effectively.

To this end, we propose **Bottom-up Policy Optimization (BuPO)**, which sequentially optimizes the internal layer policies  $\pi_{\text{Layer}}^l$  followed by the language model policy  $\pi_\theta$ :

$$\mathcal{J}_{\text{BuPO}}(\pi_\theta, \pi_{\text{Layer}}^l) = \begin{cases} \mathcal{J}_{\text{InterGRPO}}(\pi_\theta, \pi_{\text{Layer}}^l), & s_{\text{cur}} \leq s_{\text{inter}} \\ \mathcal{J}_{\text{GRPO}}(\pi_\theta), & s_{\text{cur}} > s_{\text{inter}} \end{cases} \quad (11)$$

where  $s_{\text{cur}}$  denotes the current training step, and  $s_{\text{inter}}$  specifies the number of training steps of the internal layer policy.

**Training Setup.** Using Qwen (Yang et al., 2025) and Llama (Grattafiori et al., 2024; Wang et al., 2025b) backbones, we select the last FFN layer with a positive exploration signal ( $\Delta H_{\text{FFN}}^l > 0$ ) as  $\pi_{\text{Layer}}^l$ . This assigns  $\pi_{\text{Layer}}^6$  for both Qwen3-4B and Qwen3-8B,  $\pi_{\text{Layer}}^{27}$  for Llama-OctoThinker-3B-Base, and  $\pi_{\text{Layer}}^{31}$  for Llama-OctoThinker-8B-Base. The training steps for internal layer policy are set to  $s_{\text{inter}} = 30$  for Qwen3-4B and  $s_{\text{inter}} = 20$  for the other LLMs. Refer to Appendix A.1 and A.6 for detailed algorithm and setup.

**Evaluation Setup.** We evaluate BuPO against several RL baselines, including GRPO, PPO (Sutton et al., 1998), Reinforce++ (Hu, 2025) and RLOO (Ahmadian et al., 2024). The benchmarks cover : MATH (Lightman et al., 2023), AMC23 (MAA, 2023), AIME24, and AIME25 (MAA, 2024; 2025). Due to high output variance in reasoning tasks, we report Avg@ $K$  (Pass@1 averaged over  $K$  outputs). For AIME24/25, we set  $K = 32$ , and for others  $K = 16$ . Additionally, we evaluate an unbiased Pass@ $K$  metric with  $K$  up to 256 to obtain comprehensive evaluation. Detailed evaluation setups are shown in Appendix A.6.

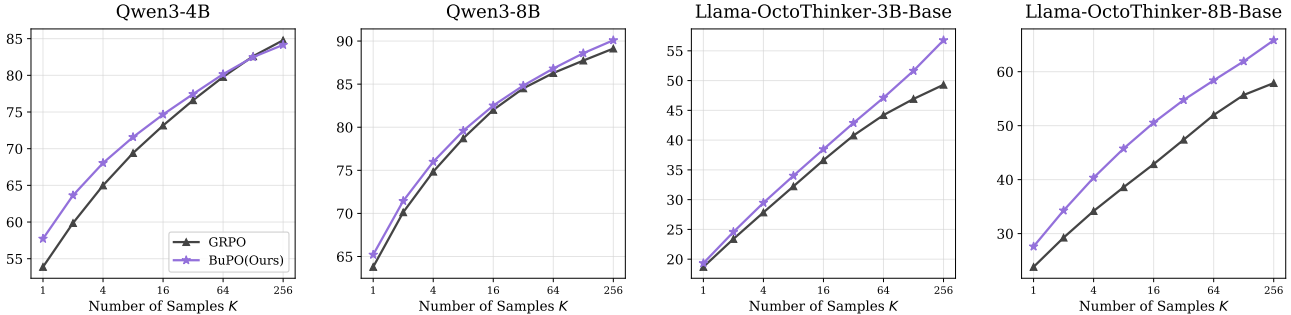
## 5.1. Main Results

As shown in Table 1, adopting the bottom-up perspective in BuPO leads to consistent Avg@ $K$  improvements over RL baseline algorithms across benchmarks and models, achieving superior average performance. On Qwen3-4B, BuPO yields gains of 4.69 points on AIME24 and 2.30 points on AIME25 compared to GRPO. Similarly, the Qwen-8B model shows improvements of 4.58 points on AIME24 and 0.76 points on AIME25. The Llama series models exhibit a similar optimization trend under BuPO, achieving an average improvement of 1.01 points on Llama-OctoThinker-3B-Base and 3.68 points on Llama-OctoThinker-8B-Base. Overall, these results suggest that aligning fine-grained internal policies in the early stages of training can effectively guide the language model policy toward improved reasoning.

For a comprehensive evaluation, we report the averaged Pass@ $K$  results of BuPO with GRPO, with  $K$  ranging from 1 to 256. As shown in Figure 6, BuPO consistently achieves a favorable trade-off across a wide range of  $K$ . On Qwen3-8B, BuPO attains the best performance for all  $K$  values, while on Qwen3-4B, the only exception occurs at  $K = 256$ . For all Llama models, BuPO achieves the best results across all  $K$  values, yielding gains of 7.48 points on Llama-OctoThinker-3B-Base and 7.93 points on Llama-OctoThinker-8B-Base in averaged

Table 1. Avg@K results on MATH500, AMC23, AIME24 and AIME25. **Bold** and underlined denote the best and second best.

Methods	AMC (Avg@16)	MATH500 (Avg@16)	AIME24 (Avg@32)	AIME25 (Avg@32)	Average
Qwen3-4B					
Vanilla	67.66	80.29	23.20	18.60	47.44
PPO	77.03	<u>83.64</u>	<u>32.60</u>	27.60	<u>55.22</u>
Reinforce++	63.44	80.63	17.40	18.65	45.03
RLOO	<u>77.66</u>	82.73	30.83	24.79	54.00
GRPO	76.88	82.41	32.19	<u>28.85</u>	55.08
BuPO	<b>81.09+4.21</b>	<b>84.90+2.49</b>	<b>36.88+4.69</b>	<b>31.15+2.30</b>	<b>58.51+3.43</b>
Qwen3-8B					
Vanilla	67.34	80.46	26.98	19.17	48.49
PPO	87.03	86.20	37.81	22.60	58.41
Reinforce++	82.66	86.05	41.77	31.15	60.41
RLOO	86.41	87.32	46.67	33.02	63.36
GRPO	85.94	<b>88.05</b>	<u>49.48</u>	<u>33.54</u>	<u>64.23</u>
BuPO	<b>89.22+3.28</b>	<u>87.76</u>	<b>54.06+4.58</b>	<b>34.38+0.76</b>	<b>66.36+2.13</b>
Llama-OctoThinker-3B-Base					
Vanilla	1.24	5.26	0.21	0.00	1.68
PPO	22.19	43.23	<u>1.04</u>	<u>0.31</u>	16.69
Reinforce++	9.38	11.59	0.00	0.10	5.27
RLOO	<u>27.03</u>	41.93	<b>2.19</b>	0.21	17.84
GRPO	<b>27.50</b>	46.07	0.63	0.10	18.58
BuPO	<b>27.50+0.00</b>	<b>49.79+3.72</b>	<u>0.63+0.00</u>	<b>0.42+0.32</b>	<b>19.59+1.01</b>
Llama-OctoThinker-8B-Base					
Vanilla	4.53	9.84	0.52	0.10	3.75
PPO	31.72	<u>56.97</u>	1.56	1.04	22.82
Reinforce++	34.69	<u>59.55</u>	<b>7.72</b>	<u>3.75</u>	<u>26.43</u>
RLOO	27.66	<u>55.97</u>	3.54	1.56	22.18
GRPO	34.84	56.89	2.50	2.19	24.11
BuPO	<b>37.66+2.82</b>	<b>62.05+5.16</b>	<u>4.69+2.19</u>	<b>6.77+4.58</b>	<b>27.79+3.68</b>

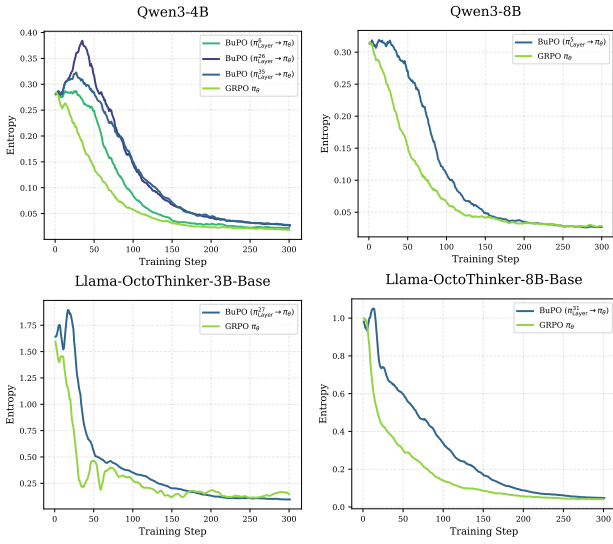

 Figure 6. Average Pass@K results on MATH500, AMC23, AIME24 and AIME25. To reduce evaluation variance, we set  $n = 300$ .

Pass@256. These results further indicate the internal policy optimization effectively enhances the reasoning capacity of  $\pi_\theta$ . We provide detailed Pass@K performance in Figure 11.

## 5.2. Analysis

**Training Dynamics of BuPO.** We further visualize the training dynamics of BuPO. As shown in Figure 7, by training the internal layer policy at an early stage, all models exhibit enhanced entropy exploration initially. For Qwen models, optimizing the first region boundary layer 6 maintains stable exploration. For Llama, we observe increased entropy during the bottom alignment stage, indicating that feature refinement in lower layers effectively provides a larger exploration space for language model policy.

**Moderate Bottom Optimization Boosts Learning.** In Sec. 4, we investigate the direct optimization of the internal layer policy. The remarkable effectiveness of this approach further validates our designed policy optimization strategy from bottom-up perspective. First, internal policy optimization at early stage compels the bottom layers to preemptively capture high-level reasoning information, establishing a better foundation for subsequent learning (Figure 5 (a,b)). Second, excessive training steps lead to model collapse, as the mismatch between the rollout policy and the optimized policy results in increased PPL (Figure 5 (c)). We conclude that moderate bottom optimization of the internal policy can further boost the learning capability of the overall language model policy, making BuPO a practical RL method.



## Impact Statement

This work aims to advance the fields of Reinforcement Learning (RL) and Mechanistic Interpretability by investigating the internal reasoning patterns of Large Language Models (LLMs). Our research contributes to the transparency of black-box LLMs by decomposing the language model policy into Internal Layer and Modular policies. By revealing how internal reasoning emerges progressively (as observed in Qwen LLMs) or abruptly (as in Llama LLMs), our work helps understand model internal mechanisms and enhances algorithmic efficiency, a crucial step toward building more controllable AI systems. Furthermore, our proposed algorithm, BuPO, improves the performance of LLMs on complex reasoning tasks, potentially enhancing the utility of AI in educational and scientific domains.

## References

Agarwal, S., Zhang, Z., Yuan, L., Han, J., and Peng, H. The unreasonable effectiveness of entropy minimization in LLM reasoning. In *Proceedings of NeurIPS*, 2025. URL <https://openreview.net/forum?id=UffTBsLgI>.

Ahmadian, A., Cremer, C., Gallé, M., Fadaee, M., Kreutzer, J., Pietquin, O., Üstün, A., and Hooker, S. Back to basics: Revisiting REINFORCE-style optimization for learning from human feedback in LLMs. In *Proceedings of ACL*, pp. 12248–12267, 2024. URL <https://aclanthology.org/2024.acl-long.662/>.

Belrose, N., Furman, Z., Smith, L., Halawi, D., Ostrovsky, I., McKinney, L., Biderman, S., and Steinhardt, J. Eliciting latent predictions from transformers with the tuned lens. *arXiv preprint arXiv:2303.08112*, 2023. URL <https://arxiv.org/abs/2303.08112>.

Brown, T., Mann, B., Ryder, N., Subbiah, M., Kaplan, J. D., Dhariwal, P., Neelakantan, A., Shyam, P., Sastry, G., Askell, A., Agarwal, S., Herbert-Voss, A., Krueger, G., Henighan, T., Child, R., Ramesh, A., Ziegler, D., Wu, J., Winter, C., Hesse, C., Chen, M., Sigler, E., Litwin, M., Gray, S., Chess, B., Clark, J., Berner, C., McCandlish, S., Radford, A., Sutskever, I., and Amodei, D. Language models are few-shot learners. In *Proceedings of NeurIPS*, volume 33, pp. 1877–1901, 2020. URL [https://proceedings.neurips.cc/paper\\_files/paper/2020/file/1457c0d6bfcb4967418bfb8ac142f64a-Paper.pdf](https://proceedings.neurips.cc/paper_files/paper/2020/file/1457c0d6bfcb4967418bfb8ac142f64a-Paper.pdf).

Cheng, D., Huang, S., Zhu, X., Dai, B., Zhao, W. X., Zhang, Z., and Wei, F. Reasoning with exploration: An entropy perspective. *arXiv preprint arXiv:2506.14758*, 2025. URL <https://arxiv.org/abs/2506.14758>.

Cui, G., Zhang, Y., Chen, J., Yuan, L., Wang, Z., Zuo, Y., Li, H., Fan, Y., Chen, H., Chen, W., et al. The entropy mechanism of reinforcement learning for reasoning language models. *arXiv preprint arXiv:2505.22617*, 2025. URL <https://arxiv.org/abs/2505.22617>.

Dai, D., Dong, L., Hao, Y., Sui, Z., Chang, B., and Wei, F. Knowledge neurons in pretrained transformers. In *Proceedings of ACL*, pp. 8493–8502, 2022. URL <https://aclanthology.org/2022.acl-long.581/>.

Dehaene, S., Kerszberg, M., and Changeux, J.-P. A neuronal model of a global workspace in effortful cognitive tasks. *Proceedings of the national Academy of Sciences*, 95(24):14529–14534, 1998. URL <https://www.pnas.org/doi/abs/10.1073/pnas.95.24.14529>.

Geva, M., Schuster, R., Berant, J., and Levy, O. Transformer feed-forward layers are key-value memories. In *Proceedings of EMNLP*, pp. 5484–5495, 2021. URL <https://aclanthology.org/2021.emnlp-main.446/>.

Geva, M., Bastings, J., Filippova, K., and Globerson, A. Dissecting recall of factual associations in auto-regressive language models. In *Proceedings of EMNLP*, pp. 12216–12235, 2023. URL <https://aclanthology.org/2023.emnlp-main.751/>.

Grattafiori, A., Dubey, A., Jauhri, A., Pandey, A., Kadian, A., Al-Dahle, A., Letman, A., Mathur, A., Schelten, A., Vaughan, A., et al. The llama 3 herd of models. *arXiv preprint arXiv:2407.21783*, 2024. URL <https://arxiv.org/abs/2407.21783>.

Guo, D., Yang, D., Zhang, H., Song, J., Wang, P., Zhu, Q., Xu, R., Zhang, R., Ma, S., Bi, X., et al. Deepseek-r1 incentivizes reasoning in llms through reinforcement learning. *Nature*, 645(8081):633–638, 2025. URL <https://www.nature.com/articles/s41586-025-09422-z>.

Gupta, A., Yeung, J., Anumanchipalli, G., and Ivanova, A. How do llms use their depth? *arXiv preprint arXiv:2510.18871*, 2025. URL <https://arxiv.org/abs/2510.18871>.

He, K., Zhang, X., Ren, S., and Sun, J. Deep residual learning for image recognition. In *Proceedings of CVPR*, pp. 770–778, 2016. URL [https://openaccess.thecvf.com/content\\_cvpr\\_2016/html/He\\_Deep\\_Residual\\_Learning\\_CVPR\\_2016\\_paper.html](https://openaccess.thecvf.com/content_cvpr_2016/html/He_Deep_Residual_Learning_CVPR_2016_paper.html).

He, Z., Liang, T., Xu, J., Liu, Q., Chen, X., Wang, Y., Song, L., Yu, D., Liang, Z., Wang, W., et al. Deepmath-103k: A large-scale, challenging, decontaminated, and

verifiable mathematical dataset for advancing reasoning. *arXiv preprint arXiv:2504.11456*, 2025. URL <https://arxiv.org/abs/2504.11456>.

Hendrycks, D., Burns, C., Kadavath, S., Arora, A., Basart, S., Tang, E., Song, D., and Steinhardt, J. Measuring mathematical problem solving with the MATH dataset. In *Proceedings of NeurIPS Datasets and Benchmarks Track*, 2021. URL <https://openreview.net/forum?id=7Bywt2mQsCe>.

Hu, J. Reinforce++: A simple and efficient approach for aligning large language models. *arXiv preprint arXiv:2501.03262*, 2025. URL <https://arxiv.org/abs/2501.03262>.

Hu, J., Zhang, Y., Han, Q., Jiang, D., Zhang, X., and Shum, H.-Y. Open-reasoner-zero: An open source approach to scaling up reinforcement learning on the base model. *arXiv preprint arXiv:2503.24290*, 2025a. URL <https://arxiv.org/abs/2503.24290>.

Hu, Y., Zhou, C., and Zhang, M. What affects the effective depth of large language models? In *Mechanistic Interpretability Workshop at NeurIPS 2025*, 2025b. URL <https://openreview.net/forum?id=ILuhAig8xo>.

Jaech, A., Kalai, A., Lerer, A., Richardson, A., El-Kishky, A., Low, A., Helyar, A., Madry, A., Beutel, A., Carney, A., et al. Openai o1 system card. *arXiv preprint arXiv:2412.16720*, 2024. URL <https://arxiv.org/abs/2412.16720>.

Jin, M., Mei, K., Xu, W., Sun, M., Tang, R., Du, M., Liu, Z., and Zhang, Y. Massive values in self-attention modules are the key to contextual knowledge understanding. In *Proceedings of ICML*, 2025. URL <https://openreview.net/forum?id=1SMcxxQiSL>.

Kwon, W., Li, Z., Zhuang, S., Sheng, Y., Zheng, L., Yu, C. H., Gonzalez, J., Zhang, H., and Stoica, I. Efficient memory management for large language model serving with pagedattention. In *Proceedings of SOSP*, pp. 611–626, 2023. URL <https://dl.acm.org/doi/abs/10.1145/3600006.3613165>.

Li, Y., Dong, Z., Sun, Y., Wang, W., Xiong, S., Luo, Y., Liu, J., Lu, H., Wang, J., Su, W., et al. Attention illuminates llm reasoning: The preplan-and-anchor rhythm enables fine-grained policy optimization. *arXiv preprint arXiv:2510.13554*, 2025. URL <https://arxiv.org/abs/2510.13554>.

Lightman, H., Kosaraju, V., Burda, Y., Edwards, H., Baker, B., Lee, T., Leike, J., Schulman, J., Sutskever, I., and Cobbe, K. Let’s verify step by step. In *Proceedings of ICLR*, 2023. URL <https://openreview.net/forum?id=v8L0pN6EOi>.

Lindsey, J., Gurnee, W., Ameisen, E., Chen, B., Pearce, A., Turner, N. L., Citro, C., Abrahams, D., Carter, S., Hosmer, B., Marcus, J., Sklar, M., Templeton, A., Bricken, T., McDougall, C., Cunningham, H., Henighan, T., Jermyn, A., Jones, A., Persic, A., Qi, Z., Thompson, T. B., Zimmerman, S., Rivoire, K., Conerly, T., Olah, C., and Batson, J. On the biology of a large language model. *Transformer Circuits Thread*, 2025. URL <https://transformer-circuits.pub/2025/attribution-graphs/biology.html>.

Liu, R., Wang, J., Shi, Y., Xie, Z., An, C., Zhang, K., Zhao, J., Gu, X., Lin, L., Hu, W., et al. Attention as a compass: Efficient exploration for process-supervised rl in reasoning models. *arXiv preprint arXiv:2509.26628*, 2025. URL <https://arxiv.org/abs/2509.26628>.

MAA. American mathematics contest 12 (amc 12), November 2023. URL [https://artofproblemsolving.com/wiki/index.php/AMC\\_12\\_Problems\\_and\\_Solutions](https://artofproblemsolving.com/wiki/index.php/AMC_12_Problems_and_Solutions).

MAA. American invitational mathematics examination (aime), February 2024. URL [https://artofproblemsolving.com/wiki/index.php/AIME\\_Problems\\_and\\_Solutions](https://artofproblemsolving.com/wiki/index.php/AIME_Problems_and_Solutions).

MAA. American invitational mathematics examination (aime), February 2025. URL [https://artofproblemsolving.com/wiki/index.php/AIME\\_Problems\\_and\\_Solutions](https://artofproblemsolving.com/wiki/index.php/AIME_Problems_and_Solutions).

Meng, K., Bau, D., Andonian, A. J., and Belinkov, Y. Locating and editing factual associations in GPT. In *Proceedings of NeurIPS*, 2022. URL <https://openreview.net/forum?id=-h6WAS6eE4>.

Meta AI. Llama 3.2: Revolutionizing edge ai and vision with open, customizable models, 2024. URL <https://huggingface.co/meta-llama>. Accessed: 2025-11-03.

nostalgebraist. interpreting gpt: the logit lens. Less-Wrong, 2020. URL <https://www.lesswrong.com/posts/AcKRB8wDpdaN6v6ru/interpreting-gpt-the-logit-lens>.

Ouyang, L., Wu, J., Jiang, X., Almeida, D., Wainwright, C., Mishkin, P., Zhang, C., Agarwal, S., Slama, K., Ray, A., Schulman, J., Hilton, J., Kelton, F., Miller, L., Simens, M., Askell, A., Welinder, P., Christiano, P. F., Leike, J., and Lowe, R. Training language models to follow instructions with human feedback. In *Proceedings of NeurIPS*, volume 35, pp. 27730–27744, 2022. URL <https://dl.acm.org/doi/10.5555/3600270.3602281>.

Peng, R., Ren, Y., Yu, Z., Liu, W., and Wen, Y. Simko: Simple pass@ k policy optimization. *arXiv preprint arXiv:2510.14807*, 2025. URL <https://arxiv.org/abs/2510.14807>.

Rafailov, R., Sharma, A., Mitchell, E., Manning, C. D., Ermon, S., and Finn, C. Direct preference optimization: Your language model is secretly a reward model. In *Proceedings of NeurIPS*, volume 36, pp. 53728–53741, 2023. URL <https://openreview.net/forum?id=HPuSIXJaa9>.

Rein, D., Hou, B. L., Stickland, A. C., Petty, J., Pang, R. Y., Dirani, J., Michael, J., and Bowman, S. R. Gpqa: A graduate-level google-proof q&a benchmark. In *First Conference on Language Modeling*, 2024. URL <https://openreview.net/forum?id=Ti67584b98>.

Shao, Z., Wang, P., Zhu, Q., Xu, R., Song, J., Bi, X., Zhang, H., Zhang, M., Li, Y., Wu, Y., et al. Deepseekmath: Pushing the limits of mathematical reasoning in open language models. *arXiv preprint arXiv:2402.03300*, 2024. URL <https://arxiv.org/abs/2402.03300>.

Sheng, G., Zhang, C., Ye, Z., Wu, X., Zhang, W., Zhang, R., Peng, Y., Lin, H., and Wu, C. Hybridflow: A flexible and efficient rlhf framework. In *Proceedings of EuroSys*, pp. 1279–1297, 2025. URL <https://dl.acm.org/doi/abs/10.1145/3689031.3696075>.

Sutton, R. S., Barto, A. G., et al. *Reinforcement learning: An introduction*, volume 1. MIT press Cambridge, 1998.

Tan, Y., He, S., Liu, K., and Zhao, J. Neural incompatibility: The unbridgeable gap of cross-scale parametric knowledge transfer in large language models. In *Proceedings of ACL*, pp. 21586–21601, 2025a. URL <https://aclanthology.org/2025.acl-long.1047/>.

Tan, Y., He, S., Liu, K., and Zhao, J. The zero-step thinking: An empirical study of mode selection as harder early exit in reasoning models. *arXiv preprint arXiv:2510.19176*, 2025b. URL <https://arxiv.org/abs/2510.19176>.

Team, K., Du, A., Gao, B., Xing, B., Jiang, C., Chen, C., Li, C., Xiao, C., Du, C., Liao, C., et al. Kimi k1. 5: Scaling reinforcement learning with llms. *arXiv preprint arXiv:2501.12599*, 2025. URL <https://arxiv.org/abs/2501.12599>.

Vaswani, A., Shazeer, N., Parmar, N., Uszkoreit, J., Jones, L., Gomez, A. N., Kaiser, L., and Polosukhin, I. Attention is all you need. In *Proceedings of NeurIPS*, pp. 6000–6010, 2017. URL <https://dl.acm.org/doi/10.5555/3295222.3295349>.

Wang, M., Li, Y., Wang, H., Zhang, X., Xu, N., Wu, B., Huang, F., Yu, H., and Mao, W. Adaptive thinking via mode policy optimization for social language agents. *arXiv preprint arXiv:2505.02156*, 2025a. URL <https://arxiv.org/abs/2505.02156>.

Wang, Z., Zhou, F., Li, X., and Liu, P. Octothinker: Mid-training incentivizes reinforcement learning scaling. *arXiv preprint arXiv:2506.20512*, 2025b. URL <https://arxiv.org/abs/2506.20512>.

Yamins, D. L. and DiCarlo, J. J. Using goal-driven deep learning models to understand sensory cortex. *Nature neuroscience*, 19(3):356–365, 2016. URL <https://www.nature.com/articles/nn.4244>.

Yang, A., Zhang, B., Hui, B., Gao, B., Yu, B., Li, C., Liu, D., Tu, J., Zhou, J., Lin, J., et al. Qwen2. 5-math technical report: Toward mathematical expert model via self-improvement. *arXiv preprint arXiv:2409.12122*, 2024. URL <https://arxiv.org/abs/2409.12122>.

Yang, A., Li, A., Yang, B., Zhang, B., Hui, B., Zheng, B., Yu, B., Gao, C., Huang, C., Lv, C., et al. Qwen3 technical report. *arXiv preprint arXiv:2505.09388*, 2025. URL <https://arxiv.org/abs/2505.09388>.

Yu, Q., Zhang, Z., Zhu, R., Yuan, Y., Zuo, X., YuYue, Dai, W., Fan, T., Liu, G., Liu, J., Liu, L., Liu, X., Lin, H., Lin, Z., Ma, B., Sheng, G., Tong, Y., Zhang, C., Zhang, M., Zhang, R., Zhang, W., Zhu, H., Zhu, J., Chen, J., Chen, J., Wang, C., Yu, H., Song, Y., Wei, X., Zhou, H., Liu, J., Ma, W.-Y., Zhang, Y.-Q., Yan, L., Wu, Y., and Wang, M. DAPO: An open-source LLM reinforcement learning system at scale. In *Proceedings of NeurIPS*, 2025. URL <https://openreview.net/forum?id=2a36EMSSTp>.

Yu, Z. and Ananiadou, S. Neuron-level knowledge attribution in large language models. In *Proceedings of EMNLP*, pp. 3267–3280, 2024. URL <https://aclanthology.org/2024.emnlp-main.191/>.

Zhang, B. and Sennrich, R. Root mean square layer normalization. In *Proceedings of NeurIPS*, volume 32, 2019. URL <https://openreview.net/pdf?id=SygkZ3MTJE>.

Zhang, H., Hao, Q., Xu, F., and Li, Y. Reinforcement learning fine-tuning enhances activation intensity and diversity in the internal circuitry of llms. *arXiv preprint arXiv:2509.21044*, 2025. URL <https://arxiv.org/abs/2509.21044>.

Zhou, Z., Yu, H., Zhang, X., Xu, R., Huang, F., Wang, K., Liu, Y., Fang, J., and Li, Y. On the role of attention heads

in large language model safety. In *Proceedings of ICLR*, 2025. URL <https://openreview.net/forum?id=h0Ak8A5yqw>.

Zhu, X., Xia, M., Wei, Z., Chen, W.-L., Chen, D., and Meng, Y. The surprising effectiveness of negative reinforcement in LLM reasoning. In *Proceedings of NeurIPS*, 2025. URL <https://openreview.net/forum?id=ftV1LG9cks>.

## A. Detailed Experiment Settings

### A.1. Implementation of BuPO

The detailed implementation of our proposed Bottom-up Policy Optimization (BuPO) algorithm is provided in Algorithm 1.

---

#### Algorithm 1 Bottom-up Policy Optimization (BuPO)

---

**Require:** Policy  $\pi_\theta$ , Dataset  $\mathcal{Q}$ , Target Layer  $l$ , Internal Training Steps  $s_{\text{inter}}$ , Total Training Steps  $S_{\text{max}}$

**Ensure:** Optimized Policy  $\pi_{\theta^*}$

```

1: Initialize training step  $s_{\text{cur}} \leftarrow 0$ .
2: while  $s_{\text{cur}} < S_{\text{max}}$  do
3:   Sample batch of prompts  $\mathbf{q} \sim \mathcal{Q}$ .
4:   Sampling: Generate  $G$  outputs  $\{\mathbf{o}_i\}_{i=1}^G$  from  $\pi_{\theta_{\text{old}}}(\cdot | \mathbf{q})$ .
5:   Evaluation: Compute rewards and advantages  $\hat{A}_{i,t}$  for each output.
6:   if  $s_{\text{cur}} \leq s_{\text{inter}}$  then
7:     Define internal policy  $\pi_{\text{Layer}}^l$  from layer  $l$  hidden states.  $\triangleright$  Phase 1: Internal Policy Optimization
8:     Compute importance ratio  $\hat{r}_{i,t} = \frac{\pi_{\text{Layer}}^l(o_{i,t} | \mathbf{q}, \mathbf{o}_{i,<t})}{\pi_{\text{Layer},\text{old}}^l(o_{i,t} | \mathbf{q}, \mathbf{o}_{i,<t})}$ .
9:     Optimize  $\pi_{\text{Layer}}^l$  maximizing  $\mathcal{J}_{\text{InterGRPO}} = \frac{1}{G} \sum_{i=1}^G \frac{1}{|\mathbf{o}_i|} \sum_t \min[\hat{r}_{i,t} \hat{A}_{i,t}, \text{clip}(\hat{r}_{i,t}, 1 - \epsilon, 1 + \epsilon) \hat{A}_{i,t}]$ .
10:    else
11:      Compute importance ratio  $\hat{r}_{i,t} = \frac{\pi_\theta(o_{i,t} | \mathbf{q}, \mathbf{o}_{i,<t})}{\pi_{\theta_{\text{old}}}(o_{i,t} | \mathbf{q}, \mathbf{o}_{i,<t})}$ .  $\triangleright$  Phase 2: Language Model Policy Optimization
12:      Optimize  $\pi_\theta$  maximizing  $\mathcal{J}_{\text{GRPO}} = \frac{1}{G} \sum_{i=1}^G \frac{1}{|\mathbf{o}_i|} \sum_t \min[\hat{r}_{i,t} \hat{A}_{i,t}, \text{clip}(\hat{r}_{i,t}, 1 - \epsilon, 1 + \epsilon) \hat{A}_{i,t}]$ .
13:    end if
14:    Update parameters  $\theta$  via gradient descent and increment  $s_{\text{cur}} \leftarrow s_{\text{cur}} + 1$ .
15: end while
output  $\pi_\theta$ 

```

---

### A.2. The Models for Experiments

We summarize all models used in our analysis and experiments in Table 3. These models are categorized into three types: Mix, Base, and Instruct.

*Table 3.* Detailed information about the selected models is provided. "Mix" refers to models that support both thinking and non-thinking modes. "Base" denotes the pre-trained model only. "Instruct" indicates models that undergo further fine-tuning based on the Base model to enhance instruction-following capabilities.

Model	Huggingface	Type	Layers
Qwen3-4B	<a href="https://huggingface.co/Qwen/Qwen3-4B">https://huggingface.co/Qwen/Qwen3-4B</a>	Mix	36
Qwen3-8B	<a href="https://huggingface.co/Qwen/Qwen3-8B">https://huggingface.co/Qwen/Qwen3-8B</a>	Mix	36
Qwen3-14B	<a href="https://huggingface.co/Qwen/Qwen3-14B">https://huggingface.co/Qwen/Qwen3-14B</a>	Mix	40
Qwen3-4B-Base	<a href="https://huggingface.co/Qwen/Qwen3-4B-Base">https://huggingface.co/Qwen/Qwen3-4B-Base</a>	Base	36
Qwen2.5-Math-7B	<a href="https://huggingface.co/Qwen/Qwen2.5-Math-7B">https://huggingface.co/Qwen/Qwen2.5-Math-7B</a>	Base	28
Qwen3-4B-Instruct-2507	<a href="https://huggingface.co/Qwen/Qwen3-4B-Instruct-2507">https://huggingface.co/Qwen/Qwen3-4B-Instruct-2507</a>	Instruct	36
Llama-3.2-3B-Instruct	<a href="https://huggingface.co/meta-llama/Llama-3.2-3B-Instruct">https://huggingface.co/meta-llama/Llama-3.2-3B-Instruct</a>	Instruct	28
Llama-3.1-8B-Instruct	<a href="https://huggingface.co/meta-llama/Llama-3.1-8B-Instruct">https://huggingface.co/meta-llama/Llama-3.1-8B-Instruct</a>	Instruct	32
Llama-OctoThinker-3B-Base	<a href="https://huggingface.co/OctoThinker/OctoThinker-3B-Long-Base">https://huggingface.co/OctoThinker/OctoThinker-3B-Long-Base</a>	Base	28
Llama-OctoThinker-8B-Base	<a href="https://huggingface.co/OctoThinker/OctoThinker-8B-Long-Base">https://huggingface.co/OctoThinker/OctoThinker-8B-Long-Base</a>	Base	32
DeepSeek-Math-7B-Base	<a href="https://huggingface.co/deepseek-ai/deepseek-math-7b-base">https://huggingface.co/deepseek-ai/deepseek-math-7b-base</a>	Base	30
DeepSeek-R1-Distill-Qwen-7B	<a href="https://huggingface.co/deepseek-ai/DeepSeek-R1-Distill-Qwen-7B">https://huggingface.co/deepseek-ai/DeepSeek-R1-Distill-Qwen-7B</a>	Instruct	28

### A.3. The Template for Experiments

We adopt the following template for all experiments involving Qwen models, building upon the Qwen-Math template used for Qwen2.5 (Yang et al., 2024) and the Qwen-Nothinking template for Qwen3.

## Qwen-Math Template

```
<|im_start|>system
Please reason step by step, and put your final answer within \boxed{ }.
<|im_end|>
<|im_start|>user
{problem}
<|im_end|>
<|im_start|>assistant
```

## Qwen3-NoThinking Template

```
<|im_start|>system
Please reason step by step, and put your final answer within \boxed{ }.
<|im_end|>
<|im_start|>user
{problem}
<|im_end|>
<|im_start|>assistant
<think>

</think>
```

For training the Llama-OctoThinker models, we adopt the original prompt in Wang et al. (2025b) to ensure performance.

## OctoThinker Template

A conversation between User and Assistant. The user asks a question, and the Assistant solves it. The assistant first thinks about the reasoning process in the mind and then provides the user with the answer. User: You must put your answer inside `\boxed{ }` and Your final answer will be extracted automatically by the `\boxed{ }` tag.

```
{problem}
Assistant:
```

#### A.4. Implementation of Internal Policy Entropy Analysis

In this section, we detail the implementation of internal policy entropy analysis. Our primary objective is to extract internal hidden states during the forward pass. In the main experiments, we evaluate model-generated responses on the MATH test set (Hendrycks et al., 2021). Entropy is computed at the token level for each layer and module, and then averaged over all generated tokens. We find that the intrinsic reasoning patterns remain stable across different tasks, e.g., commonsense question answering (Rein et al., 2024).

The computation of internal policy entropy is illustrated in the pseudo-code below. We abstract the entropy computation as a function  $\mathcal{H}(\cdot)$ . Accordingly, the entropy change of the internal layer policy is defined as:

$$\Delta H_{\text{Layer}}^l = \mathcal{H}(\mathbf{H}^l) - \mathcal{H}(\mathbf{H}^{l-1}). \quad (12)$$

For the two core Transformer submodules, the entropy changes are computed separately. Specifically, for the self-attention module, we define:

$$\Delta H_{\text{ATTN}}^l = \mathcal{H}(\mathbf{A}^l) - \mathcal{H}(\text{LN}(\mathbf{H}^{(2l-2)})), \quad (13)$$

and for the feed-forward network (FFN), we define:

$$\Delta H_{\text{FFN}}^l = \mathcal{H}(\mathbf{F}^l) - \mathcal{H}(\text{LN}(\mathbf{H}^{(2l-1)})). \quad (14)$$

These definitions allow us to quantify how each layer and submodule contributes to the evolution of the internal policy entropy.

**Calculation of Internal Policy Entropy (PyTorch Implementation)**

```

# Get layer hidden states by register hook
hidden_state = get_from_hook()

# Compute logits as the same as original forward
logits = self.model.lm_head(hidden_state)

# Apply softmax for normalization
probs = torch.softmax(logits, dim=-1)

# Apply log_softmax for speedy computation
log_probs = torch.log_softmax(logits, dim=-1)

# Calculate internal layer policy
entropies = -(probs * log_probs).sum(dim=-1)
    
```

**Discussion: Comparison to the Logit Lens.** Notably, our definition of internal policy differs from the logit lens approach (nostalgebraist, 2020), particularly in how layer normalization (LN) is handled. To clarify this distinction, we provide a systematic comparison between the two formulations in Table 4.

Our definition adopts a policy-centric perspective, treating the internal hidden states as an explicitly samplable policy. In contrast, the logit lens is primarily designed to project hidden states into the discrete vocabulary space in order to inspect the most likely output tokens at intermediate layers. We intentionally omit LN based on empirical considerations: in our experiments, incorporating LN leads to unstable entropy dynamics and reduced interpretability.

Extensive analyses and experiments with BuPO further demonstrate that our formulation of internal policy serves as a robust interpretability tool for uncovering internal reasoning mechanisms in LLMs.

Table 4. Comparison of logits lens with our definition of internal policy.

	Logit Lens	Internal Policy
Perspective	Discrete Token	Samplable Policy
Definition	$\text{LN}(\mathbf{H}^l) \mathbf{E}_u^T$	$\text{softmax}(\mathbf{H}^l \mathbf{E}_u^T)$
Trainable	✗	✓

### A.5. Implementation of Internal Policy Optimization

In internal policy optimization, namely InterGRPO, at each optimization step, we select a specific internal layer  $l$  and optimize its internal policy  $\pi_{\text{Layer}}^l$ , defined as  $\pi_{\text{Layer}}^l = \text{softmax}(\mathbf{H}^l \mathbf{E}_u^T)$ , where  $\mathbf{H}^l$  is the hidden states at layer  $l$ . The gradient flow for internal policy optimization is determined by the residual structure of the Transformer, where the hidden state  $\mathbf{H}^l$  is a function of all parameters from layer 1 to  $l$ , but is independent of parameters in higher layers.

Formally, for any parameter  $\theta_k$  in layer  $k$ , the gradient of the InterGRPO loss with respect to  $\theta_k$  can be expressed using the chain rule:

$$\frac{\partial J_{\text{InterGRPO}}(\pi_{\text{Layer}}^l)}{\partial \theta_k} = \frac{\partial J_{\text{interGRPO}}}{\partial \pi_{\text{Layer}}^l} \cdot \frac{\partial \pi_{\text{Layer}}^l}{\partial \mathbf{H}^l} \cdot \frac{\partial \mathbf{H}^l}{\partial \theta_k} \quad (15)$$

Due to the residual connections,  $\frac{\partial \mathbf{H}^l}{\partial \theta_k} \neq 0$  only when  $k \leq l$ , and is zero otherwise. Thus, the gradients for different layers can be summarized as:

$$\frac{\partial J_{\text{InterGRPO}}(\pi_{\text{Layer}}^l)}{\partial \theta_k} = \begin{cases} \frac{\partial J_{\text{interGRPO}}}{\partial \pi_{\text{Layer}}^l} \cdot \frac{\partial \pi_{\text{Layer}}^l}{\partial \mathbf{H}^l} \cdot \frac{\partial \mathbf{H}^l}{\partial \theta_k}, & \text{if } k \leq l \\ 0, & \text{if } k > l \end{cases} \quad (16)$$

This means that, during InterGRPO optimization for layer  $l$ , only the parameters of layers 0 through  $l$  and unembedding matrix  $\mathbf{E}_u$  are updated, while all higher layers ( $k > l$ ) remain unaffected. This targeted gradient flow ensures that internal policy optimization provides direct supervision to the selected layer and all lower layers, strengthening foundational reasoning capabilities without interfering with higher-level representations.

**Training Setup.** Based on the findings in Sec. 3, we select Qwen3-4B (Yang et al., 2025) in non-thinking mode for investigation. For the training set, we randomly sample 5k entries from *DeepMath-103k* (He et al., 2025). We train the models using the verl framework (Sheng et al., 2025). The prompt batch size is 128, with 8 rollouts generated per prompt. The sampling temperature during training is set to 1.0, and the maximum context length is set to 9,216 tokens. We update the model with a mini-batch size of 32 for 300 steps and a learning rate of 1e-6. For Qwen3-4B, the region boundaries identified in Sec. 3.2 lie at layers 6 and 26. Additionally, we focus on aligning the internal policy of the penultimate layer, which is critical for the final prediction. Accordingly, we compare the internal policies  $\pi_{\text{Layer}}^6$ ,  $\pi_{\text{Layer}}^{26}$ , and  $\pi_{\text{Layer}}^{35}$  optimized via InterGRPO, against the overall policy  $\pi_\theta$  optimized with GRPO (He et al., 2025).

## A.6. Implementation of Main Experiments

**Detailed Training Setup.** Specifically, we focus on the Qwen3 series, which maintain a stable EIC pattern, using Qwen3-4B and Qwen3-8B (Yang et al., 2025). Meanwhile, we select Llama-OctoThinker-3B-Base and Llama-OctoThinker-8B-Base from the Llama series, as these models demonstrate improved training behavior after mid-training based on Llama-3.2-Base (Wang et al., 2025b). We implement GRPO and other baseline algorithms using the veRL framework (Sheng et al., 2025). Across all algorithms and model variants, we adopt a unified set of hyperparameters, as reported in Table 5, and do not employ entropy regularization or KL-based losses. For PPO, the critic network is trained separately with a learning rate of  $1 \times 10^{-5}$ .

**Evaluation Setup.** We use vLLM (Kwon et al., 2023) with temperature 1.0 and top\_p 1.0. This metric is defined as  $\text{Pass}@K := \mathbb{E}_{x \sim \mathcal{D}} [1 - \binom{n-c}{K} / \binom{n}{K}]$ , where  $c$  denotes the number of correct completions out of  $n$  generated responses. To reduce evaluation variance on those datasets, we set  $n = 300$ .

Table 5. RL Hyperparameters

Hyperparameter	Value
Optimizer	AdamW
Policy learning rate	$1e^{-6}$
Critic learning rate	$1e^{-5}$ (for PPO)
Training batch size	128 prompts
Samples per prompt	8
Mini-batch size	32 prompts
Policy updates per rollout	16
Max prompt length	1024 tokens
Max response length	7168 tokens (Qwen) / 3072 (Llama)
Rollout temperature	1.0
Clip range $\epsilon$	0.2

## B. Extended Experiment Results

### B.1. Internal Policy Entropy Dynamics for More Models

In this section, we present additional preliminary analyses of internal policy entropy dynamics across a broader set of models. Specifically, we examine different variants of the same backbone, including Base, Instruct, and Mix versions, as well as models trained with supervised fine-tuning (SFT) and reinforcement learning (RL). In addition, we include the DeepSeek-Math model (He et al., 2025) to further enrich the comparative analysis.

**Further Training Has Limited Impact on Internal Reasoning Patterns.** We further analyze models that undergo additional training beyond standard pre-training. Specifically, we include DeepSeek-R1-Distill-Qwen-7B, which is further trained from Qwen2.5-Math-7B using distilled responses from Guo et al. (2025) with SFT, as well as Llama-OctoThinker-3B-Base and Llama-OctoThinker-8B-Base, which are obtained via continued pre-training (i.e., mid-training) based on Llama-3.2-3B-Base and Llama-3.2-8B-Base, respectively (Wang et al., 2025b). Moreover, Qwen3-4B and Qwen3-4B-Base also show consistent pattern after post-training with RL. Notably, these additional training procedures exhibit only marginal influence on the internal reasoning patterns.

In summary, reinforcement learning, supervised fine-tuning, and mid-training do not substantially alter the model’s internal reasoning mechanisms, suggesting that these intrinsic patterns are primarily determined by the model architecture and initial pre-training. Understanding how such patterns emerge remains an important direction for future work.

**Same Series of Models Exhibit Consistent Structures.** After analyzing in all analysis plots across models, we find that same series of model show consistent structures. For instance, all Qwen3 series models shows progressive internal reasoning pattern including Qwen3-4B, Qwen3-8B and Qwen3-14B, also with other base or instruct version. Also, Llama-3.1 and Llama-3.2 show intra-difference and inter-consistency.

**Entropy Dynamics of DeepSeek-Math.** We further analyze the internal reasoning mechanisms of DeepSeek-Math-7B-Base to provide a more comprehensive comparison. As illustrated in Figure 9, DeepSeek-Math-7B-Base exhibits a markedly different entropy dynamics: the overall internal policy entropy decreases substantially and converges primarily in the middle layers. This phenomenon is primarily driven by the consistently negative entropy change in the FFN module, i.e.,  $\Delta H_{\text{FFN}}^l < 0$ , as illustrated in Figure 10, particularly in the middle layers.

Based on this observation, we infer that both Qwen and DeepSeek-Math demonstrate strong capability in knowledge absorption during post-training, indicating that convergence behavior in internal reasoning plays a critical role in effective learning, in contrast to Llama. Moreover, the generation search space of DeepSeek-Math appears more constrained than that of Qwen, particularly the Qwen3 series, suggesting reduced exploration capacity. We hypothesize that such internal reasoning patterns significantly influence the effectiveness of further training, pointing to promising directions for architectural design and optimization of foundation models.

### B.2. How do Internal modules influence the residual stream?

To further understand how internal modules shape the residual stream in Qwen models with progressive reasoning pattern, we analyze residual cosine similarity, which quantifies how each module writes to the residual pathway (Hu et al., 2025b). For a given layer  $l$ , we compute  $\text{cossim}(\mathbf{A}^l, \mathbf{H}^{l-1})$  for self-attention and  $\text{cossim}(\mathbf{F}^l, \mathbf{H}^{l-1} + \mathbf{A}^l)$  for the FFN. A cosine similarity near zero indicates writing new, orthogonal features; negative values indicate feature suppression; and positive

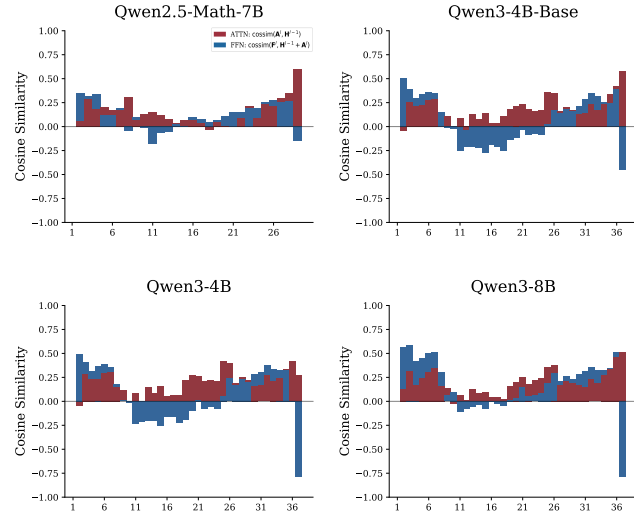


Figure 8. Residual cosine similarity across different Qwen models

17

values indicate amplification of existing features.

As shown in Figure 8, the Qwen models largely follow the entropy dynamics discussed earlier, while exhibiting clear inter-generation differences. For Qwen3, self-attention consistently amplifies the residual stream, in line with its positive entropy change and expanded exploration behavior. In contrast, Qwen2.5 shows noticeably weaker attention write-in strength, with reduced cosine similarity magnitudes, consistent with its negative entropy change in self-attention.

The FFN modulates the residual stream in a stage-dependent manner across all models: in lower layers, it injects largely orthogonal features to support exploration; in middle layers, it suppresses vague signals while integrating parametric knowledge in FFN, corresponding to the Integration stage; and in upper layers, it amplifies and integrates features to drive convergence. Across all models, the final layer exhibits a sharp directional shift, underscoring its critical role in final prediction (Gupta et al., 2025; Agarwal et al., 2025).

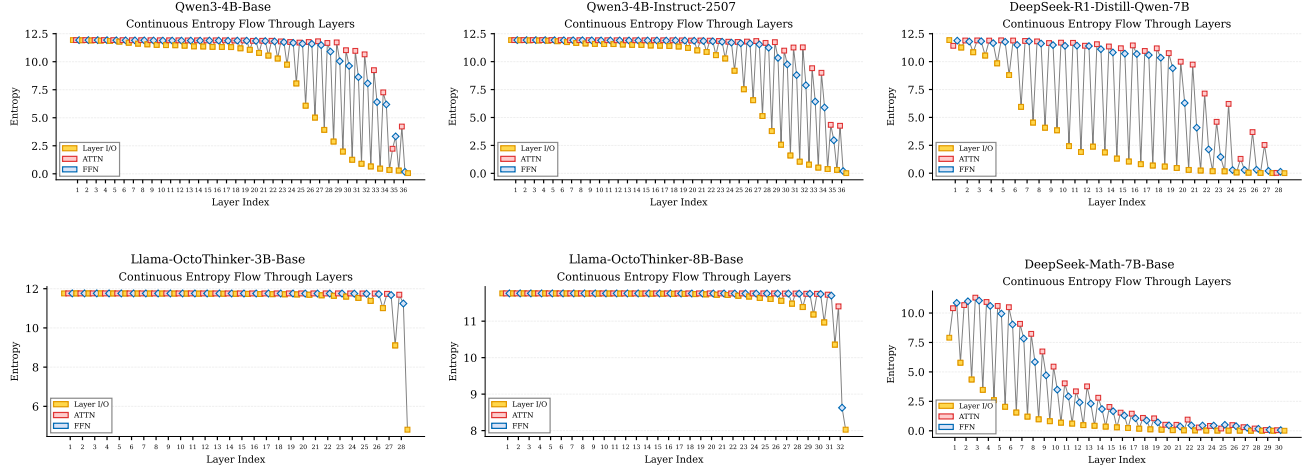


Figure 9. Continuous entropy dynamics of internal policy for additional models. The information flows from  $\mathbf{H}^{l-1}$  into  $\mathbf{A}^l, \mathbf{F}^l$ , then to the next layer  $\mathbf{H}^l$ .

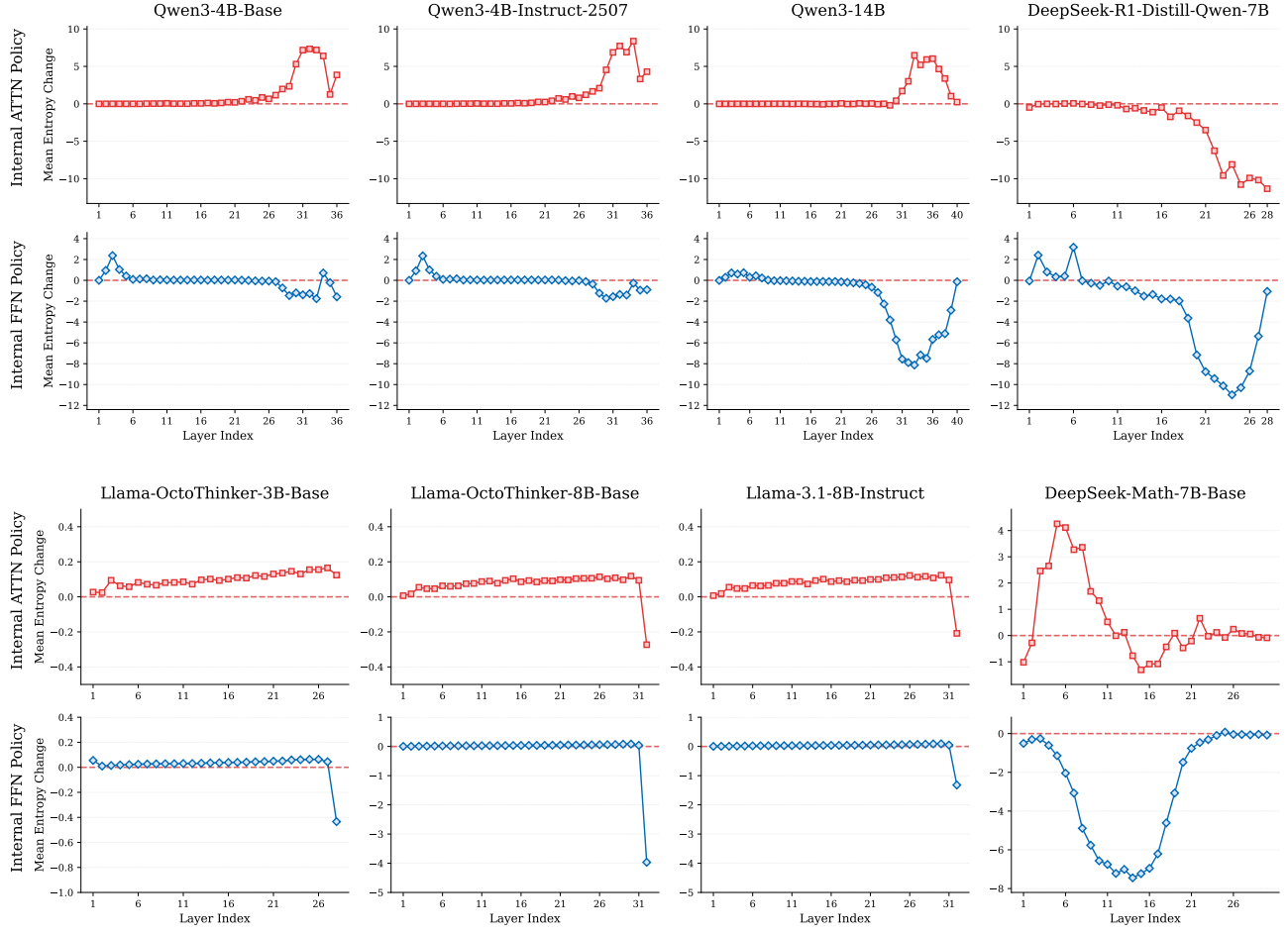


Figure 10. Entropy change dynamics of internal policy with more models.

### B.3. Pass@K Performance across Datasets

We further provide a detailed version of Figure 6 across AMC23, MATH500, AIME24, and AIME25. Our proposed BuPO consistently outperforms the vanilla GRPO baseline.

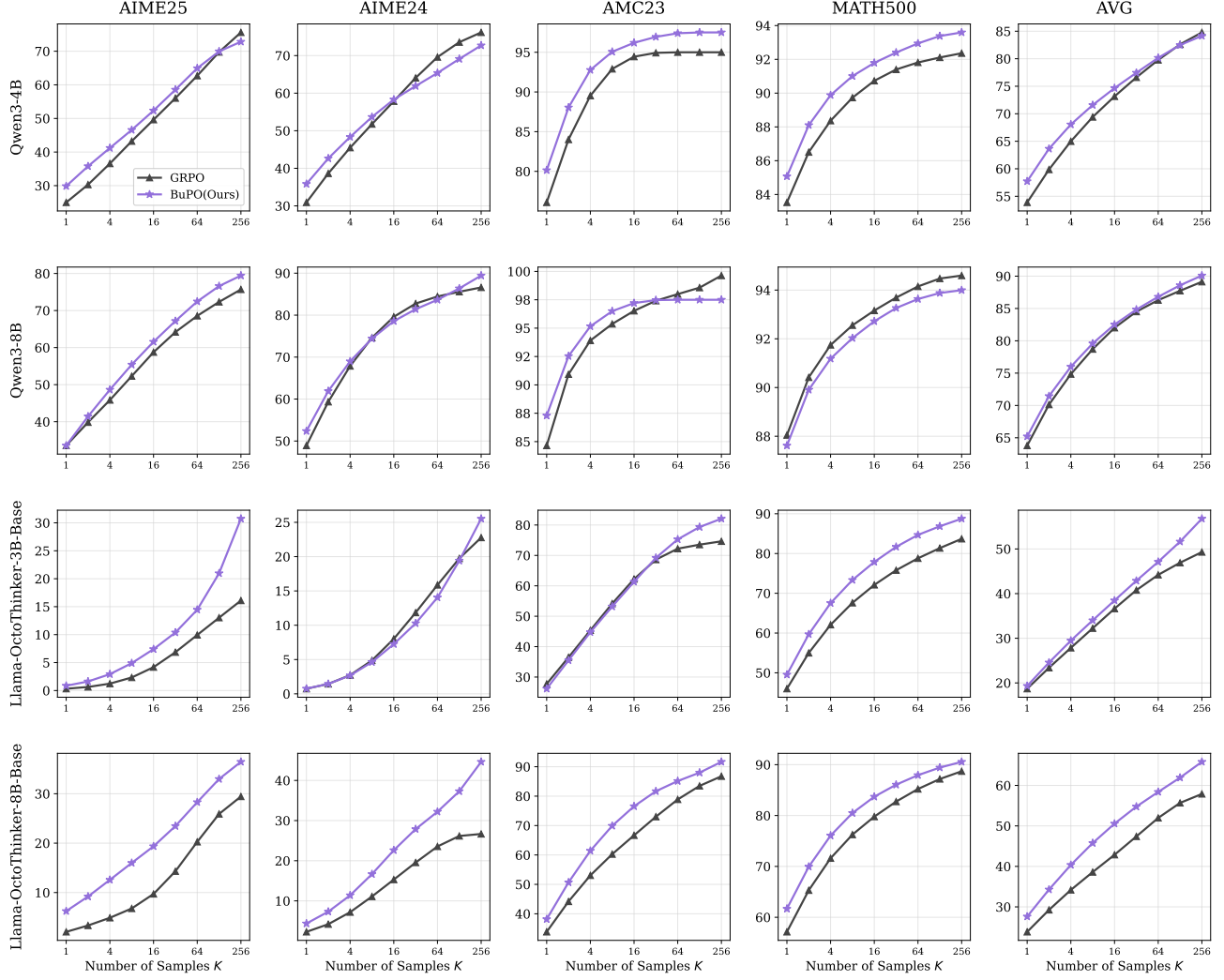


Figure 11. Pass@K results on MATH500, AMC23, AIME24 and AIME25. To reduce evaluation variance, we set  $n = 300$ .